Magnetic-Field Manipulation of Chemical Bonding in Artificial Molecules

CONSTANTINE YANNOULEAS, UZI LANDMAN

School of Physics, Georgia Institute of Technology, Atlanta, Georgia 30332-0430

ABSTRACT: The effect of orbital magnetism on the chemical bonding of lateral, two-dimensional artificial molecules is studied in the case of a 2e double quantum dot (artificial molecular hydrogen). It is found that a perpendicular magnetic field reduces the coupling (tunneling) between the individual dots and, for sufficiently high values, it leads to complete dissociation of the artificial molecule. The method used is building on Löwdin's work on projection operators in quantum chemistry; it is a spin-and-space unrestricted Hartree–Fock method in conjunction with the companion step of the restoration of spin and space symmetries via projection techniques (when such symmetries are broken). This method is able to describe the full range of couplings in two-dimensional double quantum dots, from the strong-coupling regime exhibiting delocalized molecular orbitals to the weak-coupling and dissociation regimes associated with a generalized valence bond combination of atomic-type orbitals localized on the individual dots. © 2002 Wiley Periodicals, Inc. Int J Quantum Chem 90: 699–708, 2002

Key words: orbital magnetism; 2e double quantum dot; coupling; projection operators; delocalized molecular orbitals

Introduction

Two-dimensional (2D) quantum dots (QDs) [1, 2] are usually referred to as artificial atoms, a term suggestive of strong similarities between these manmade nanodevices and the physical behavior of natural atoms. As a result, in the last few years, an intensive theoretical effort [2–13] has been devoted toward the elucidation of the appropriate analogies and/or differences. Recently, we showed

[10–12] that in the absence of a magnetic field the most promising analogies are mainly found outside the confines of the central-field approximation underlying the independent-particle model and the ensuing physical picture of electronic shells and the Aufbau Principle. Indeed, as a result of the lower electronic densities in QDs, strong e–e correlations can lead (as a function of the ratio R_W between the interelectron repulsion and the zero-point kinetic energy) to a drastically different physical regime, where the electrons become localized, arranging themselves in concentric geometric shells and forming electron molecules (referred to also as Wigner molecules in analogy to Wigner crystallization [14] in infinite media). In this context, it was found

[11, 12] that the proper analogy for the particular case of a $2e$ QD is the collective-motion picture reminiscent of the fleeting and rather exotic phenomena of the doubly excited natural helium atom, where the emergence of a "floppy" trimeric molecule (consisting of the two localized electrons and the heavy α-particle nucleus) has been well established [15, 16].

A natural extension [10, 13, 17–23] of this theoretical effort has also developed in the direction of 2D QD molecules (QDMs, often referred to as artificial molecules), aiming at elucidating the analogies and differences between such artificially fabricated [24, 25] molecular nanostrustures and natural molecules. (Depending on the arrangement of the individual dots, two classes of QDMs can be distinguished: lateral [10, 13, 17–24] and vertical [22, 23, 25] ones.)

In a previous article [21] and for the case of zero magnetic field (field-free case), we addressed the interplay of coupling and dissociation in lateral QDMs. We showed that this interplay relates directly to the nature of the coupling in the artificial molecules, and in particular to the question whether such coupling can be described by the molecular orbital (MO) theory or the valence bond (VB) theory in analogy with the chemical bond in natural molecules.

A major attraction of QDs and QDMs is the fact that, due to their larger size and different materials parameters (i.e., electron effective mass and dielectric constant), the full range of orbital magnetic effects can be covered for magnetic-field values easily attainable in the laboratory (<45 T). This range extends from the weak-field perturbative regime (Zeeman orbital splitting and perturbative diamagnetism) to the intense-field regime exhibiting a substantial spatial distortion of single-particle electronic orbitals. This behavior contrasts with the case of natural atoms and molecules for which magnetic fields of sufficient strength (i.e., $>10^5$ T) for the production of novel phenomena [26, 27] related to orbital magnetism beyond the perturbative regime are known to occur only in astrophysical environments, e.g., on the surfaces of neutron stars. In this article, we study the effect of orbital magnetism on the interdot coupling in a lateral, two-electron double quantum dot. This nanodevice represents an artificial analog to the natural hydrogen molecule and can be denoted as H_2-QDM. It has been suggested [19] that it can function as the elemental two-qubit logic gate in quantum computing.

We find that the interplay of the MO versus the VB description provides the proper framework for understanding the influence of orbital magnetism on the chemical bonding of the H_2-QDM. In particular, we show that a perpendicular magnetic field reduces the coupling between the individual dots and, for sufficiently high values, it leads to the dissociation of the artificial molecule. As a result, in addition to the obvious parameters of interdot barrier height and interdot separation, the magnetic field supplies a third variable able to induce dissociation and thus to control the strength of the interdot coupling.

Our approach is twofold. As a first step, we utilize a self-consistent-field theory which can go beyond the MO approximation, namely the spin-and-space unrestricted Hartree–Fock (sS-UHF), which was introduced by us [10, 11] for the description of the many-body problem of both single [10, 11] and molecular [10] QDs. The equations used are given in Ref. [28], where they are simply referred to as unrestricted Hartree–Fock (UHF); the additional sS labeling employed by us emphasizes the range of possible symmetry unrestrictions in the solutions of these equations. In particular, the sS-UHF differs from the more familiar restricted HF (RHF) in two ways: (i) *it relaxes the double-occupancy requirement—namely, it employs different spatial orbitals for the two different (i.e., the up and down) spin directions* [thus the designation "spin (s) unresricted"], and (ii) *it relaxes the requirement that the electron orbitals be constrained by the symmetry of the external confining field* [thus the designation "space (S) unrestricted"]. Since it is a general property [29] of the HF equations to preserve at each iteration step the symmetries of the many-body hamiltonian (whenever they happen to be present in the HF electron density), the input trial density at the initial step must be constructed in such a way as to a priori reflect the relaxation of the two requirements mentioned above. Observe further that, in order to describe electron localization, the sS-UHF employs fully the fact that all N (where N is the number of electrons) orbital-dependent effective (mean-field) HF potentials can be different from each other.

We remark that within the terminology adopted here, the simple designation Hartree–Fock (HF) in the literature most often refers to our RHF, in particular in atomic physics and the physics of the homogeneous electron gas. In nuclear physics, however, the simple designation HF most often refers to a space (S)-UHF. The simply designated UHF as used in chemistry (e.g., in calculations of open shell

molecules) corresponds most often to our s-UHF (but not simultaneously space unrestricted HF).

As a second step, we will show that, in conjunction with Löwdin's spin-projection technique [30, 31], the solutions with broken space symmetry allowed in QDMs by the sS-UHF provide a natural vehicle for formulating a generalized valence bond (GVB) referred to also as a generalized Heitler–London (GHL), theory. This approach allows us to describe the chemical bonding in artificial molecules in both the case of an applied magnetic field and the field-free case.

The Two-Center-Oscillator Confining Potential

In the 2D two-center oscillator* (TCO), the single-particle levels associated with the confining potential of the artificial molecule are determined by the single-particle hamiltonian [32, 33]

$$H = T + \frac{1}{2}m^*\omega_{xk}^2 x^2 + \frac{1}{2}m^*\omega_{yk}^2 y_k'^2 + V_{\text{neck}}(y) + h_k$$
$$+ \frac{g^*\mu_B}{\hbar}\mathbf{B}\cdot\mathbf{s}, \quad (1)$$

where $y_k' = y - y_k$ with $k = 1$ for $y < 0$ (left) and $k = 2$ for $y > 0$ (right), and the h_k's control the relative well-depth, thus allowing studies of hetero-QDMs. x denotes the coordinate perpendicular to the interdot axis (y). $T = (\mathbf{p} - e\mathbf{A}/c)^2/2m^*$, with $\mathbf{A} = 0.5(-By, Bx, 0)$, and the last term in Eq. (1) is the Zeeman interaction with g^* being the effective g factor, μ_B the Bohr magneton, and $\mathbf{s}$ the spin of an individual electron. Here we limit ourselves to systems with $\hbar\omega_{x1} = \hbar\omega_{x2} = \hbar\omega_x$. The most general shapes described by H are two semiellipses connected by a smooth neck [$V_{\text{neck}}(y)$]. $y_1 < 0$ and $y_2 > 0$ are the centers of these semiellipses, $d = y_2 - y_1$ is the interdot distance, and m^* is the effective electron mass.

For the smooth neck, we use $V_{\text{neck}}(y) = \frac{1}{2}m^*\omega_{yk}^2[c_k y_k'^3 + d_k y_k'^4]\theta(|y| - |y_k|)$, where $\theta(u) = 0$ for $u > 0$ and $\theta(u) = 1$ for $u < 0$. The four constants c_k and d_k can be expressed via two parameters, as follows: $(-1)^k c_k = (2 - 4\epsilon_k^b)/y_k$ and $d_k = (1 - 3\epsilon_k^b)/y_k^2$, where the barrier-control parameters $\epsilon_k^b = (V_b - h_k)/V_{0k}$ are related to the actual (controlable) height of the bare barrier (V_b) between the two QDs, and $V_{0k} = m^*\omega_{yk}^2 y_k^2/2$ (for $h_1 = h_2$, $V_{01} = V_{02} = V_0$).

*A 3D magnetic-field-free version of the TCO has been used in the description of fission in metal clusters [32] and atomic nuclei [33].

The single-particle levels of H, including an external perpendicular magnetic field B, are obtained by numerical diagonalization in a (variable-with-separation) basis consisting of the eigenstates of the auxiliary hamiltonian:

$$H_0 = \frac{\mathbf{p}^2}{2m^*} + \frac{1}{2}m^*\omega_x^2 x^2 + \frac{1}{2}m^*\omega_{yk}^2 y_k'^2 + h_k. \quad (2)$$

This eigenvalue problem is separable in x and y; i.e., the wave functions are written as $\Phi_{m\nu}(xy) = X_m(x)Y_\nu(y)$. The solutions for $X_m(x)$ are those of a one-dimensional oscillator, and for $Y_\nu(y)$ they can be expressed through the parabolic cylinder functions [32, 33] $U[\alpha_k, (-1)^k \xi_k]$, where $\xi_k = y_k'\sqrt{2m^*\omega_{yk}/\hbar}$, $\alpha_k = (-E_y + h_k)/(\hbar\omega_{yk})$, and $E_y = (\nu + 0.5)\hbar\omega_{y1} + h_1$ denote the y-eigenvalues. The matching conditions at $y = 0$ for the left and right domains yield the y-eigenvalues and the eigenfunctions $Y_\nu(y)$ (m is integer and ν is in general real).

In this article, we will limit ourselves to symmetric (homopolar) QDMs, i.e., $\hbar\omega_x = \hbar\omega_{y1} = \hbar\omega_{y2} = \hbar\omega_0$, with equal well-depths of the left and right dots, i.e., $h_1 = h_2 = 0$. In all cases, we will use $\hbar\omega_0 = 5$ meV and $m^* = 0.067m_e$ (this effective-mass value corresponds to GaAs).

The Many-Body Hamiltonian

The many-body hamiltonian $\mathcal{H}$ for a dimeric QDM comprising N electrons can be expressed as a sum of the single-particle part $H(i)$ defined in Eq. (1) and the two-particle interelectron Coulomb repulsion,

$$\mathcal{H} = \sum_{i=1}^{N} H(i) + \sum_{i=1}^{N}\sum_{j>i}^{N} \frac{e^2}{\kappa r_{ij}}, \quad (3)$$

where κ is the dielectric constant and r_{ij} denotes the relative distance between the i and j electrons.

As we mentioned in the Introduction, we will use the sS-UHF method for determining at a first level an approximate solution of the many-body problem specified by the hamiltonian (3). The sS-UHF equations are solved in the Pople–Nesbet–Roothaan formalism [28] using the interdot-distance adjustable basis formed with the eigenfunctions $\Phi_{m\nu}(x, y)$ of the TCO defined previously.

As we will explicitly illustrate for the case of the H_2-QDM, the next step in improving the sS-UHF solution involves the use of projection techniques in relation to the UHF single Slater determinant.

Artificial Molecular Hydrogen (H_2-QDM) in a Magnetic Field: A Generalized Valence Bond Approach

THE sS-UHF DESCRIPTION

As an introductory example to the process of symmetry breaking in HF, we consider in this subsection the field-free ($B = 0$) case of H_2-QDM with $\kappa = 20$ (this value is an intermediate one to the three different values of κ that will be considered below in the case of an applied magnetic field). Figure 1 displays the RHF and sS-UHF results for the $P = N_\alpha - N_\beta = 0$ case (singlet) and for an interdot distance $d = 30$ nm and an interdot barrier $V_b = 4.95$ meV (α and β denote up and down spins, respectively). In the RHF (Fig. 1, left), both the spin-up and spin-down electrons occupy the same bonding (σ_g) molecular orbital. In contrast, the sS-UHF results exhibit breaking of the spatial reflection symmetry; namely, the spin-up electron occupies an optimized* $1s$ atomiclike orbital (AO) in the left QD, while the spin-down electron occupies the corresponding $1s'$ AO in the right QD. Concerning the total energies, the RHF yields $E_{RHF}(P = 0) = 13.68$ meV, while the sS-UHF energy is $E_{sSUHF}(P = 0) = 12.83$, representing a gain in energy of 0.85 meV. Since the energy of the triplet is $E_{sUHF}(P = 2) = E_{sSUHF}(P = 2) = 13.01$ meV, the sS-UHF singlet conforms to the requirement [34] that for two electrons at zero magnetic field the singlet is always the ground state; on the other hand the RHF MO solution fails in this respect.

PROJECTED WAVE FUNCTION AND RESTORATION OF THE BROKEN SYMMETRY

To make further progress, we utilize the spin-projection technique to restore the broken symmetry of the sS-UHF determinant (henceforth we will drop the prefix sS when referring to the sS-UHF determinant),

$$\sqrt{2}\Psi_{UHF}(1, 2) = \begin{vmatrix} u(\mathbf{r}_1)\alpha(1) & v(\mathbf{r}_1)\beta(1) \\ u(\mathbf{r}_2)\alpha(2) & v(\mathbf{r}_2)\beta(2) \end{vmatrix}$$
$$\equiv |u(1)\bar{v}(2)\rangle, \qquad (4)$$

where $u(\mathbf{r})$ and $v(\mathbf{r})$ are the $1s$ (left) and $1s'$ (right) localized orbitals of the sS-UHF solution. An example of such orbitals for the field-free case is displayed

---

*The optimized orbitals are anisotropic (i.e., noncircularly symmetric), reflecting polarization effects due to the electronic interdot interaction.
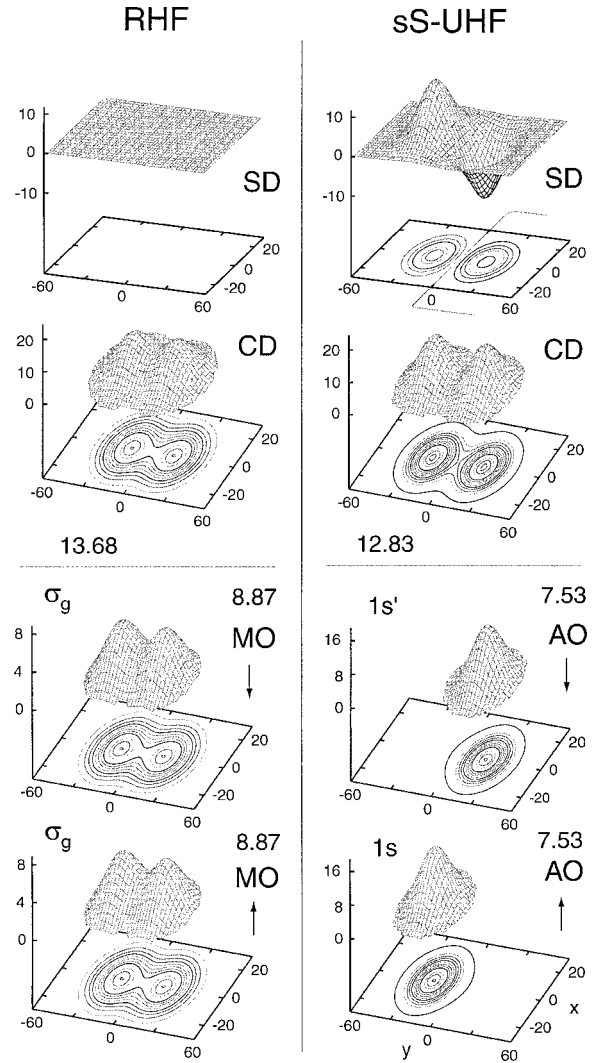

FIGURE 1. Lateral H_2-QDM at zero magnetic field: Occupied orbitals (modulus square, bottom half) and total charge (CD) and spin (SD) densities (top half) for the $P = 0$ spin unpolarized case. Left column: RHF results. Right column: sS-UHF results exhibiting a breaking of the space symmetry. The numbers displayed with each orbital are their eigenenergies in meV, while the up and down arrows indicate an electron with an up or down spin. The numbers displayed with the charge densities are the total energies in meV. Unlike the RHF case, the spin density of the sS-UHF exhibits a well developed spin density wave. Distances are in nm and the electron densities in 10^{-4} nm^{-2}. The choice of parameters is $m^* = 0.067 m_e$, $\hbar\omega_0 = 5$ meV, $d = 30$ nm, $V_b = 4.95$ meV, $\kappa = 20$.

in the right column of Figure 1. Similar localized orbitals appear also in the $B \neq 0$ case, so that in general the functions $u(\mathbf{r})$ and $v(\mathbf{r})$ are complex. α and β denote the up and down spin functions, respectively.

In Eq. (4) we also define a compact notation for the Ψ_{UHF} determinant, where a bar over a space orbital denotes a spin-down electron; absence of a bar denotes a spin-up electron.

$\Psi_{UHF}(1, 2)$ is an eigenstate of the projection S_z of the total spin $\mathbf{S} = \mathbf{s}_1 + \mathbf{s}_2$, but not of S^2. One can generate a many-body wave function which is an eigenstate of S^2 with eigenvalue $s(s + 1)\hbar^2$ by applying the projection operator introduced by Löwdin [30, 31],

$$P_s \equiv \prod_{s' \neq s} \frac{S^2 - s'(s' + 1)\hbar^2}{[s(s + 1) - s'(s' + 1)]\hbar^2}, \qquad (5)$$

where the index s' runs over the quantum numbers of S^2.

The result of S^2 on any UHF determinant can be calculated with the help of the expression

$$S^2 \Phi_{UHF} = \hbar^2 \left[(N_\alpha - N_\beta)^2/4 + N/2 + \sum_{i<j} \varpi_{ij} \right] \Phi_{UHF}, \qquad (6)$$

where the operator ϖ_{ij} interchanges the spins of electrons i and j provided that their spins are different; N_α and N_β denote the number of spin-up and spin-down electrons, respectively, while N denotes the total number of electrons.

For the singlet magnetic state of two electrons $(N = 2)$, one has $N_\alpha = N_\beta = 1$, $S_z = 0$, and S^2 has only the two quantum numbers $s = 0$ and $s = 1$. As a result,

$$2\sqrt{2}P_0 \Psi_{UHF}(1, 2) = (1 - \varpi_{12})\sqrt{2}\Psi_{UHF}(1, 2)$$
$$= |u(1)\bar{v}(2)\rangle - |\bar{u}(1)v(2)\rangle. \qquad (7)$$

In contrast to the single-determinantal wave functions of the RHF and sS-UHF methods, the projected many-body wave function (7) is a linear superposition of two Slater determinants and thus represents a corrective step beyond the mean-field approximation.

Expanding the determinants in Eq. (7), one finds the equivalent expression

$$2P_0 \Psi_{UHF}(1, 2) = \left(u(\mathbf{r}_1)v(\mathbf{r}_2) + u(\mathbf{r}_2)v(\mathbf{r}_1)\right)\chi(0, 0), \qquad (8)$$

where the spin eigenfunction is given by

$$\chi(s = 0;\ S_z = 0) = \left(\alpha(1)\beta(2) - \alpha(2)\beta(1)\right)/\sqrt{2}. \qquad (9)$$

Equation (8) has the form of a Heitler–London (HL) [35] or valence bond* [36, 37] wave function for the singlet magnetic state. However, unlike

the HL scheme which uses the orbitals $\phi_L(\mathbf{r})$ and $\phi_R(\mathbf{r})$ of the separated (left and right) atoms,[†] expression (8) employs the sS-UHF orbitals which are self-consistently optimized for any separation d, potential barrier height V_b, and magnetic field B. As a result, expression (8) can be characterized as a GVB[‡] (also termed GHL) wave function. Taking into account the normalization of the spatial part, we arrive at the following improved wave function for the singlet state exhibiting all the symmetries of the original many-body hamiltonian (here, the spatial reflection symmetry is automatically restored along with the spin symmetry),

$$\Psi_{GVB}^s(1, 2) = n_s \sqrt{2} P_0 \Psi_{UHF}(1, 2), \qquad (10)$$

where the normalization constant is given by

$$n_s^2 = 1/(1 + S_{uv}S_{vu}), \qquad (11)$$

S_{uv} being the overlap integral of the $u(\mathbf{r})$ and $v(\mathbf{r})$ orbitals (which are complex in the presence of a magnetic field $\mathbf{B}$),

$$S_{uv} = \int u^*(\mathbf{r})v(\mathbf{r})\, d\mathbf{r}. \qquad (12)$$

The total energy of the GVB state is given by

$$E_{GVB}^s = n_s^2[h_{uu} + h_{vv} + S_{uv}h_{vu} + S_{vu}h_{uv} + J_{uv} + K_{uv}], \qquad (13)$$

tween the atomic symbols denoting a shared electron. Later in 1927 Heitler and London formulated the first quantum mechanical theory of the pair-electron bond for the case of the hydrogen molecule. The theory was subsequently developed by Pauling and others in the 1930s into the modern theory of the chemical bond called the *Valence Bond Theory*.

†References [19, 20] have studied, as a function of the magnetic field, the behavior of the singlet–triplet splitting of the H_2-QDM by diagonalizing the two-electron hamiltonian inside the minimal four-dimensional basis formed by the products $\phi_L(\mathbf{r}_1)\phi_L(\mathbf{r}_2)$, $\phi_L(\mathbf{r}_1)\phi_R(\mathbf{r}_2)$, $\phi_R(\mathbf{r}_1)\phi_L(\mathbf{r}_2)$, $\phi_R(\mathbf{r}_1)\phi_R(\mathbf{r}_2)$ of the $1s$ orbitals of the *separated* QDs. This Hubbard-type method [19] (as well as the refinement employed by Ref. [20] of enlarging the minimal two-electron basis to include the p orbitals of the separated QDs) is an improvement over the simple HL method (see Ref. [19]), but apparently it is only appropriate for the weak-coupling regime at sufficiently large distances and/or interdot barriers. In addition this method fails explicitly (it yields a triplet ground state at $B = 0$ [19]) for small values of κ. Our method is free of such limitations, since we employ here an interdot-distance adjustable basis of at least 70 spatial TCO molecular orbitals when solving for the sS-UHF ones. Even with consideration of the symmetries, this amounts to calculating a large number of two-body Coulomb matrix elements, of the order of 10^6.

‡More precisely our GVB method belongs to a class of projection techniques known as variation *before* projection, unlike the familiar in chemistry GVB method of Goddard and co-workers (Goddard III, W. A.; Dunning, Jr., T. H.; Hunt, W. J.; Hay, P. J. Acc Chem Res 1973, 6, 368), which is a variation *after* projection (see Ref. [29]).

*The early empirical electronic model of valence was primarily developed by G. N. Lewis who introduced a symbolism where an electron was represented by a dot (e.g., H:H) with a dot be-

where h is the single-particle part (1) of the total hamiltonian (3), and J and K are the direct and exchange matrix elements associated with the e–e repulsion $e^2/\kappa r_{12}$. For comparison, we give also here the corresponding expression for the total energy of the HF "singlet" (i.e., the determinant with $S_z = 0$), either in the RHF ($v = u$, no spin contamination) or the sS-UHF (spin-contaminated) case,

$$E_{\mathrm{HF}}^{\mathrm{s}} = h_{uu} + h_{vv} + J_{uv}. \qquad (14)$$

For the triplet with $S_z = \pm 1$, the projected wave function coincides with the original HF determinant, so that the corresponding energies in all three approximation levels are equal; i.e., $E_{\mathrm{GVB}}^{\mathrm{t}} = E_{\mathrm{RHF}}^{\mathrm{t}} = E_{\mathrm{UHF}}^{\mathrm{t}}$.

COMPARISON OF RHF, sS-UHF, AND GVB RESULTS

In this section, we study in detail the behavior of the interdot coupling in the H$_2$-QDM in the presence of a perpendicular magnetic field. We present numerical results for three values of the dielectric constant, namely, $\kappa = 45$ (e–e repulsion much weaker than the case of GaAs), $\kappa = 25$ (e–e repulsion weaker than the GaAs case), and $\kappa = 12.9$ (case of GaAs). In particular we study the evolution of the energy difference, $\Delta\varepsilon = E^{\mathrm{s}} - E^{\mathrm{t}}$, between the singlet and the triplet states as a function of an increasing magnetic field varying from $B = 0$ to $B = 9$ T. The evolution of the two occupied sS-UHF orbitals of the singlet state is illustrated by plotting them at the two end values, $B = 0$ and $B = 9$ T. In all three figures (i.e., Figs. 2, 3, and 4), the lower half corresponds to a vanishing interdot barrier $V_b = 0$ (unified deformed dot at $B = 0$), while the upper half corresponds to a finite value of V_b, thus being closer to the notion of a molecule proper. The interdot distance is chosen to be $d = 30$ nm in all three cases.

Case of $\kappa = 45$

Figure 2 displays the evolution of $\Delta\varepsilon$ as a function of the magnetic field for $\kappa = 45$ and for all three approximation levels, i.e., the RHF (MO theory, top solid line), the sS-UHF (dashed line), and the GVB (lower solid line). (The same convention for the $\Delta\varepsilon(B)$ curves is followed throughout this article.) The case of $V_b = 0$ is shown at the bottom panel, while the case of $V_b = 3.71$ meV is displayed in the top panel. The insets display as a function of B the overlap (modulus square, $|S_{uv}|^2$) of the two orbitals $u(\mathbf{r})$ and $v(\mathbf{r})$ of the singlet state. In this calculation, the effective g factor was set equal to zero,
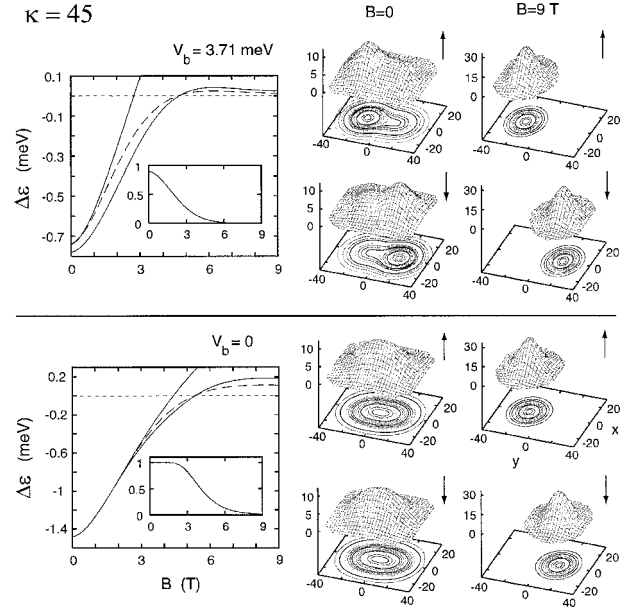

FIGURE 2. Lateral H$_2$-QDM in the presence of a magnetic field and for $\kappa = 45$: The left column displays the energy difference $\Delta\varepsilon$ between the singlet and triplet states according to the RHF (MO theory, upper solid line), the sS-UHF (dashed line), and the GVB approach (projection method, lower solid line) as a function of the applied magnetic field B. The two other columns display the sS-UHF spin-up ($\uparrow$) and spin-down ($\downarrow$) occupied orbitals (modulus square) of the singlet state for $B = 0$ (field-free case, middle column) and $B = 9$ T (right column). The top half corresponds to a bare interdot barrier of $V_b = 3.71$ meV, while the bottom half describes the no barrier case $V_b = 0$. For $B = 9$ T complete dissociation has been practically reached. The choice of the remaining parameters is $m^* = 0.067m_e$, $\hbar\omega_0 = 5$ meV, $d = 30$ nm, and $g^* = 0$. Distances are in nm and the orbital densities in 10^{-4} nm^{-2}. Insets: The overlap integral (modulus square) of the two orbitals of the singlet state as a function of B.

$g^* = 0$, so that the gain of energy due to the Zeeman effect does not obstruct for large B the convergence of $\Delta\varepsilon$ toward zero. Due to its smallness relative to $\hbar\Omega_{\mathrm{eff}} = \hbar(\omega_0^2 + \omega_c^2/4)^{1/2}$ (where $\omega_c = eB/m^*c$ is the cyclotron frequency), the actual Zeeman contribution can simply be added to the result calculated for $g^* = 0$.

We observe first that as a function of B, for both the $V_b = 0$ and the $V_b = 3.71$ meV cases and for all three levels of approximation, the $\Delta\varepsilon$ energy difference starts from a minimum negative value (singlet ground state) and progressively increases to zero; after crossing the zero value, it remains positive (triplet ground state). However, for large values of

B there is a sharp contrast in the behavior of the RHF curves compared to the sS-UHF and GVB ones. Indeed after crossing the zero axis, the RHF curves incorrectly continue to rise sharply and very early they move outside the range of values plotted here (at $B = 9$ T, the RHF values are 0.93 and 1.21 meV for $V_b = 0$ and 3.71 meV, respectively). In contrast, after reaching a broad maximum, the positive $\Delta\varepsilon$ branches of both the sS-UHF and GVB curves converge to zero for sufficiently large values of B.

The convergence of the singlet and triplet total energies to the same value indicates that the H_2-QDM dissociates as B attains sufficiently large values. This is also reflected in the behavior of the overlaps (see insets) as a function of the magnetic field. In fact, the overlaps decrease practically to zero as a function of B, suggesting that the two corresponding orbitals $u(\mathbf{r})$ and $v(\mathbf{r})$ of the singlet state tend to become strongly localized on the individual dots.

The molecular dissociation induced by the magnetic field and the associated electron localization is further demonstrated by an examination of the orbital densities (orbitals modulus square) themselves. These densities are plotted for both the end values of $B = 0$ (field-free case, middle column) and $B = 9$ T (strong magnetic field, right column). For $B = 9$ T, it is apparent that the plots portray orbitals well localized on the individual dots. In contrast, for $B = 0$ the orbitals are clearly delocalized over the entire QDM. In particular, for $B = 0$ and $V_b = 0$ the two orbitals $u(\mathbf{r})$ and $v(\mathbf{r})$, which are different in general, have collapsed to the same $1s$-type distorted orbital associated with the single-particle picture of a unified deformed dot.

One effect of choosing a very weak e–e repulsion ($\kappa = 45$) is that in the $V_b = 0$ case the three levels of approximation collapse to the same MO value (no symmetry breaking) for magnetic fields below $B < 2.9$ T, a fact that is also reflected in the orbitals themselves (see the $B = 0$ case in the middle column of the lower half of Fig. 2). However, for $V_b = 3.71$ meV, even such a weak e–e repulsion does not suffice to inhibit symmetry breaking in the field-free case. As a result, for $B = 0$ and $V_b = 3.71$ meV, the two $u(\mathbf{r})$ and $v(\mathbf{r})$ orbitals, although spread out over the entire molecule, are clearly different and the GVB singlet lies lower in energy than the corresponding MO value.

A second observation is that both the sS-UHF and the GVB solutions describe the dissociation limit ($\Delta\varepsilon \to 0$) for sufficiently large B rather well. In addition in both the sS-UHF and the GVB methods the

singlet state at $B = 0$ remains the ground state for all values of the interdot barrier. Between the two singlets, the GVB one is always the lowest, and as a result the GVB method presents an improvement over the sS-UHF method both at the level of symmetry preservation and at the level of energetics. Furthermore, whether a singlet or triplet, the GVB always results in a stabilization of the ground state; the improved behavior of the GVB over the sS-UHF holds for all values of κ.

We note that the failure of the MO (RHF) approximation to describe the dissociation process induced by the magnetic field is similar to its failure to describe dissociation of the molecule in the field-free case as a function of the interdot barrier and distance (see Ref. [21]). As discussed in Ref. [21], due to the underlying MO picture, the spin-density functional calculations of Refs. [17, 18] also fail to describe the molecular dissociation process in the field-free case.* Such spin-density functional calculations are expected to fail in the presence of a magnetic field as well.

Case of $\kappa = 25$

The influence of the magnetic field on the properties of the H_2-QDM in the case of a stronger e–e repulsion ($\kappa = 25$) is described in Figure 3. Again we set $g^* = 0$ for the same reasons as in the previous case; the meaning of $\Delta\varepsilon$ and of the displayed orbitals is the same as in Figure 2. Compared to

---

*Symmetry breaking in coupled QDs within the local spin density (LSD) approximation has been explored by Kolehmainen, J.; Reimann, S. M.; Koskinen, M.; Manninen, M. Eur Phys J D 2000, 13, 731. However, unlike the HF case for which a fully developed theory for the restoration of symmetries has long been established (see, e.g., Ref. [29]), the breaking of space symmetry within the spin-dependent density functional theory poses a serious dilemma (Perdew, J. P.; Savin, A.; Burke, K. Phys Rev A 1995, 51, 4531). This dilemma has not been fully resolved todate; several remedies (like projection, ensembles, etc.) are being proposed, but none of them appears to be completely devoid of inconsistencies (Savin, A. Recent Developments and Applications of Modern Density Functional Theory; Seminario, J. M., Ed.; Elsevier: Amsterdam, 1996; p. 327). In addition, due to the unphysical self-interaction error, the density-functional theory is more resistant against symmetry breaking (see Bauernschmitt, R.; Ahlrichs, R. J Chem Phys 1996, 104, 9047) than the sS-UHF, and thus it fails to describe a whole class of broken symmetries involving electron localization, e.g., the formation at $B = 0$ of Wigner molecules in QDs (see footnote 7 in Ref. [10]), the hole trapping at Al impurities in silica (Laegsgaard, J.; Stokbro, K. Phys Rev Lett 2001, 86, 2834), or the interaction driven localization–delocalization transition in d- and f-electron systems, like plutonium (Savrasov, S. Y.; Kotliar, G.; Abrahams, E. Nature 2001, 410, 793).
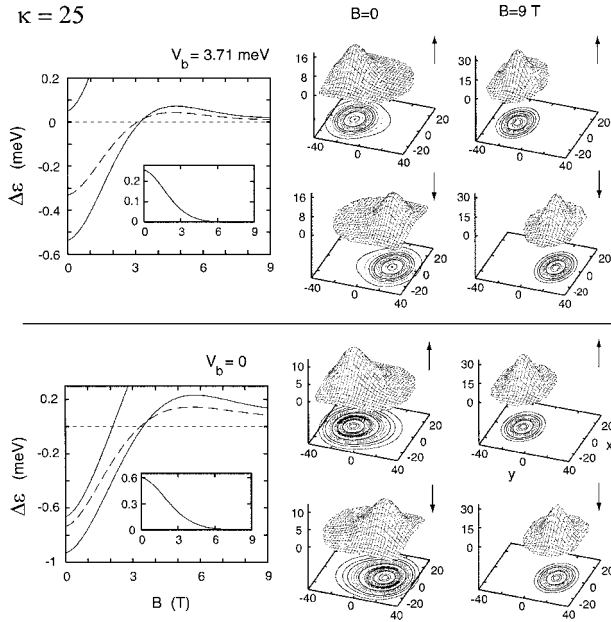
$\kappa = 25$

FIGURE 3. Lateral H_2-QDM in the presence of a magnetic field and for $\kappa = 25$: The left column displays the energy difference $\Delta\varepsilon$ between the singlet and triplet states according to the RHF (MO theory, upper solid line), the sS-UHF (dashed line), and the GVB approach (projection method, lower solid line) as a function of the applied magnetic field B. The two other columns display the sS-UHF spin-up ($\uparrow$) and spin-down ($\downarrow$) occupied orbitals (modulus square) of the singlet state for $B = 0$ (field-free case, middle column) and $B = 9$ T (right column). The top half describes the case of a bare interdot barrier of $V_b = 3.71$ meV, while the bottom half describes the no barrier case $V_b = 0$. For $B = 9$ T complete dissociation has been practically reached. The choice of the remaining parameters is $m^* = 0.067m_e$, $\hbar\omega_0 = 5$ meV, $d = 30$ nm, and $g^* = 0$. Distances are in nm and the orbital densities are in 10^{-4} nm^{-2}. Insets: The overlap integral (modulus square) of the two orbitals of the singlet state as a function of B.

the $\kappa = 45$ case, the increase of the e–e repulsion is accompanied by an overall strengthening of symmetry breaking and electron localization, since there is no range of parameters for which the sS-UHF and GVB solutions collapse into the symmetry-adapted MO (RHF) one. Indeed, even for $V_b = 0$ the three levels of approximation provide different values for the singlet–triplet difference $\Delta\varepsilon$, with the GVB solution yielding in the field-free case the highest stabilization for the singlet. For $V_b = 3.71$ meV, the MO solution fails outright even in the field-free case for which it predicts a positive $\Delta\varepsilon$ (triplet ground state) in violation of the theorem stating [34] that

the ground state of a $2e$ system at $B = 0$ is always a singlet.

The overall strengthening of electron localization is also reflected in the behavior of the overlap integrals (see insets), since now they start at $B = 0$ with smaller values compared to the corresponding values of the $\kappa = 45$ case. In addition, the trend toward stronger electron localization with smaller κ can be further confirmed by an inspection of the orbitals of the singlet state displayed in the middle ($B = 0$) and right ($B = 9$ T) columns of Figure 3. Compared to the corresponding orbitals in Figure 2, this trend is obvious and we will not describe it in detail. It will suffice to stress only that, whatever the degree of initial electron localization at $B = 0$, the applied magnetic field enhances even further this localization, achieving again a practically complete dissociation of the artificial molecule at $B = 9$ T.

Case of $\kappa = 12.9$ (GaAs)

The dielectric constant for a GaAs heterointerface is $\kappa = 12.9$, which corresponds to a further increase in the e–e repulsion compared to the two previous cases of $\kappa = 45$ and $\kappa = 25$. This case is presented in Figure 4. Note that here the Zeeman contribution has been included from the beginning by taking g^* to be equal to its actual value in the GaAs heterointerfaces; i.e., $g^* = -0.44$. As a result, the sS-UHF and GVB curves for $\Delta\varepsilon$ converge to a straight line representing the Zeeman linear dependence γB (with $\gamma \approx 0.026$ meV/T for $S_z = +1$, short dashed line) instead of vanishing for large B.

The results presented in Figure 4 confirm again the trend that electron localization becomes stronger the stronger the interelectron repulsion. As we found previously, the proper description of this strong electron localization requires consideration of symmetry breaking via the sS-UHF (long dashed curve in the $\Delta\varepsilon$ vs. B plots) and the subsequent construction of GVB wave functions via projection techniques (solid curve in the $\Delta\varepsilon$ vs. B plots). The MO description is outright wrong, since the corresponding $\Delta\varepsilon$ values are positive in the whole interval $0 \leq B \leq 9$ T; in fact they are so large that the whole MO curves lie outside the plotted ranges in Figure 4. For $B = 9$ T, and in both the barrierless ($V_b = 0$) case and the case with an interdot barrier of $V_b = 4.94$ meV, the artificial molecule has practically dissociated. Compared to the previous cases of $\kappa = 45$ and $\kappa = 25$, the molecule starts with a stronger electron localization already in the field-free case and with increasing B it moves much faster toward complete dissociation.
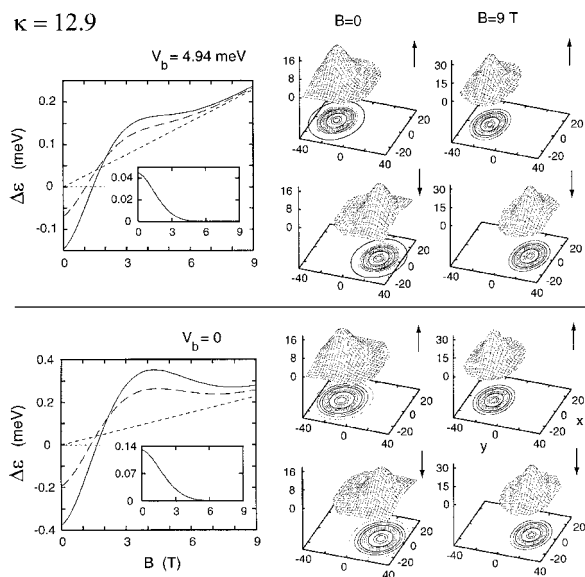
FIGURE 4. Lateral H_2-QDM in the presence of a magnetic field and for $\kappa = 12.9$ (GaAs): The left column displays the energy difference $\Delta\varepsilon$ between the singlet and triplet states according to the sS-UHF (long dashed line) and the GVB approach (projection method, solid line) as a function of the applied magnetic field B. The two other columns display the sS-UHF spin-up ($\uparrow$) and spin-down ($\downarrow$) occupied orbitals (modulus square) of the singlet state for $B = 0$ (field-free case, middle column) and $B = 9$ T (right column). The top half describes the case of a bare interdot barrier of $V_b = 4.94$ meV, while the bottom half describes the no barrier case $V_b = 0$. For $B = 9$ T complete dissociation has been practically reached. The choice of the remaining parameters is $m^* = 0.067 m_e$, $\hbar\omega_0 = 5$ meV, $d = 30$ nm, and $g^* = -0.44$ (GaAs). Distances are in nm and the orbital densities are in 10^{-4} nm^{-2}. Insets: The overlap integral (modulus square) of the two orbitals of the singlet state as a function of B.

Overview of Common Trends in the Singlet–Triplet Energy Difference

According to the GVB calculations, the common trend that can be seen in all cases (independent of the value of κ) is that the singlet–triplet energy difference is initially negative (singlet ground state) in the field-free case. With increasing magnetic field, this energy difference becomes larger (diminishes in absolute value), crosses the value of zero at a certain B_0, and remains positive (triplet ground state) for all $B \geq B_0$, converging from above to the straight line representing the Zeeman contribution (or to zero if the Zeeman contribution is neglected). This means that for sufficiently large val-

ues of B the singlet–triplet energy difference is given simply by the Zeeman energy and that the molecule has practically dissociated. The trend toward dissociation is reached faster the stronger the e–e repulsion.

It is interesting to note again that for $\kappa = 45$ (weaker e–e repulsion) the sS-UHF and GVB solutions collapse to the MO solution for values of the magnetic field smaller than $B \leq 2.9$ meV. However, for the stronger e–e repulsions ($\kappa = 25$ and $\kappa = 12.9$) the sS-UHF and GVB solutions remain energetically well below the MO solution. Since the separation considered here ($d = 30$ nm) is a rather moderate one (compared to the value $l_0 = 28.50$ nm at $B = 0$ for the extent of the 1s lowest orbital of an individual dot with $\hbar\omega_0 = 5$ meV), we conclude that there is a large range of materials parameters, interdot distances, and magnetic-field values for which the QDMs are weakly coupled and cannot be described by the MO theory; a similar conclusion was reached in Ref. [21] for the field-free case.

Conclusions

We have shown that, even in the presence of an applied magnetic field, the sS-UHF method, in conjunction with the companion step of the restoration of symmetries when such symmetries are broken, is able to describe the full range of couplings in a QDM, from the strong-coupling regime exhibiting delocalized molecular orbitals to the weak-coupling one associated with Heitler–London-type combinations of atomic orbitals.

The breaking of space symmetry within the sS-UHF method is necessary in order to properly describe the weak-coupling and dissociation regimes of QDMs. The breaking of the space symmetry produces optimized atomiclike orbitals localized on each individual dot. Further improvement is achieved with the help of projection techniques which restore the broken symmetries and yield multideterminantal many-body wave functions. The method of the restoration of symmetry was explicitly illustrated for the case of the H_2-QDM in the presence of a magnetic field. It led to the introduction of a generalized valence bond many-body wave function as the appropriate vehicle for the description of the weak-coupling and dissociation regimes of artificial molecules.

Additionally, we showed that the RHF, whose orbitals preserve the space symmetries and are delocalized over the whole molecule, is naturally associ-

ated with the molecular orbital theory. In a generalization of the field-free case of natural [36–38] and artificial [21] molecules, it was found that the RHF fails to describe the weak-coupling and dissociation regimes of QDMs in the presence of an applied magnetic field as well.

References

1. Kastner, M. A. Phys Today 1993, 46, 24; Ashoori, R. C. Nature 1996, 379, 413; Kouwenhoven, L. P.; Marcus, C. M.; McEuen, P. L.; Tarucha, S.; Westervelt, R. M.; Wingreen, N. S. Mesoscopic Electron Transport; Sohn, L. L.; Kouwenhoven, L. P.; Schoen, G., Eds.; Kluwer: Dordrecht, 1997; p. 105.

2. Chakraborty, T. Quantum Dots: A Survey of the Properties of Artificial Atoms; Elsevier: Amsterdam, 1999.

3. Pfannkuche, D.; Gudmundsson, V.; Maksym, P. A. Phys Rev B 1993, 47, 2244.

4. Hawrylak, P.; Pfannkuche, D. Phys Rev Lett 1993, 70, 485.

5. Ferconi, M.; Vignale, G. Phys Rev B 1994, 50, 14722.

6. Hirose, K.; Wingreen, N. S. Phys Rev B 1999, 59, 4604.

7. Lee, I. H.; Rao, V.; Martin, R. M.; Leburton, J. P. Phys Rev B 1998, 57, 9035.

8. Austing, D. G.; Sasaki, S.; Tarucha, S.; Reimann, S. M.; Koskinen, M.; Manninen, M. Phys Rev B 1999, 60, 11514.

9. Maksym, P. A.; Imamura, H.; Mallon, G. P.; Aoki, H. J Phys Condens Matter 2000, 12, R299.

10. Yannouleas, C.; Landman, U. Phys Rev Lett 1999, 82, 5325; ibid. 2000, 85, 2220(E).

11. Yannouleas, C.; Landman, U. Phys Rev B 2000, 61, 15895.

12. Yannouleas, C.; Landman, U. Phys Rev Lett 2000, 85, 1726.

13. Barnett, R. N.; Cleveland, C. L.; Häkkinen, H.; Luedtke, W. D.; Yannouleas, C.; Landman, U. European Phys J D 1999, 9, 95.

14. Wigner, E. Phys Rev 1934, 46, 1002.

15. Kellman, M. E.; Herrick, D. R. J Phys B 1978, 11, L755; Phys Rev A 1980, 22, 1536; Kellman, M. E. Int J Quantum Chem 1997, 65, 399.

16. Yuh, H.-J.; Ezra, G.; Rehmus, P.; Berry, R. S. Phys Rev Lett 1981, 47, 497; Ezra, G. S.; Berry, R. S. Phys Rev A 1983, 28, 1974; Berry, R. S. Contemp Phys 1989, 30, 1.

17. Nagaraja, S.; Leburton, J. P.; Martin, R. M. Phys Rev B 1999, 60, 8759.

18. Wensauer, A.; Steffens, O.; Suhrke, M.; Rössler, U. Phys Rev B 2000, 62, 2605.

19. Burkard, G.; Loss, D.; DiVincenzo, D. P. Phys Rev B 1999, 59, 2070.

20. Hu, X.; Das Sarma, S. Phys Rev A 2000, 61, 062301.

21. Yannouleas, C.; Landman, U. European Phys J D 2001, 16, 373 (ArXiv: cond-mat/0107014).

22. Palacios, J. J.; Hawrylak, P. Phys Rev B 1995, 51, 1769.

23. Partoens, B.; Peeters, F. M. Phys Rev Lett 2000, 84, 4433; Pi, M.; Emperador, A.; Barranco, M.; Garcias, F.; Muraki, K.; Tarucha, S.; Austing, D. G. Phys Rev Lett 2001, 87, 066801.

24. Waugh, F. R.; Berry, M. J.; Mar, D. J.; Westervelt, R. M.; Campman, K. L.; Gossard, A. C. Phys Rev Lett 1995, 75, 705; Blick, R. H.; Pfannkuche, D.; Haug, R. J.; von Klitzing, K.; Eberl, K. Phys Rev Lett 1998, 80, 4032.

25. Schmidt, T.; Haug, R. J.; von Klitzing, K.; Forster, A.; Lüth, H. Phys Rev Lett 1997, 78, 1544; Austing, D. G.; Honda, T.; Muraki, K.; Tokura, Y.; Tarucha, S. Physica B 1998, 251, 206.

26. Ruder, H.; Wunner, G.; Herold, H.; Geyer, H. Atoms in Strong Magnetic Fields; Springer-Verlag: Berlin, 1994.

27. Lai, D.; Salpeter, E. E. Phys Rev A 1996, 53, 152; Kravchenko, Yu. P.; Liberman, M. A. Phys Rev A 1998, 57, 3403; Lai, D. Rev Mod Phys 2001, 73, 629.

28. See (a) Section 3.8.4 in Szabo, A; Ostlund, N. S. Modern Quantum Chemistry; McGraw–Hill: New York, 1989; (b) Pople, J. A.; Nesbet, R. K. J Chem Phys 1954, 22, 571.

29. Ring, P.; Schuck, P. The Nuclear Many-Body Problem; Springer: New York, 1980; Chaps. 5.5 and 11.

30. Löwdin, P. O. Phys Rev B 1955, 97, 1509; Rev Mod Phys 1964, 36, 966.

31. Pauncz, R. The Construction of Spin Eigenfunctions: An Exercise Book; Kluwer Academic/Plenum: New York, 2000.

32. Yannouleas, C.; Landman, U. J Phys Chem 1995, 99, 14577; Yannouleas, C.; Barnett, R. N.; Landman, U. Comments At Mol Phys 1995, 31, 445.

33. Maruhn, J.; Greiner, W. Z Phys 1972, 251, 431; Wong, C. Y. Phys Lett 1969, 30B, 61.

34. Mattis, D. C. The Theory of Magnetism, Springer Series in Solid-State Sciences No. 17; Springer: New York, 1988; Vol. I, Sec. 4.5.

35. Heitler, H.; London, F. Z Phys 1927, 44, 455.

36. Coulson, C. A. Valence; Oxford University Press: London, 1961.

37. Murrell, J. N.; Kettle, S. F.; Tedder, J. M. The Chemical Bond; Wiley: New York, 1985.

38. See Section 3.8.7 in Ref. [28a].